Article:
Frood, R, Palkhi, E, Barnfield, M et al. (3 more authors) (2018) Can MR textural analysis improve the prediction of extracapsular nodal spread in patients with oral cavity cancer? European Radiology, 28 (12). pp. 5010-5018. ISSN 0938-7994

https://doi.org/10.1007/s00330-018-5524-x

Can MR Textural Analysis Improve Detection of Extracapsular Nodal Spread in Patients with Oral Cavity Cancer?

Russell Frood[a], Ebrahim Palkhi[a], Mark Barnfield[b], Robin Prestwich[c], Sriram Vaidyanathan[a], Andrew Scarsbrook[a,d]

a) Department of Nuclear Medicine, Leeds Teaching Hospitals NHS Trust, UK
b) Department of Medical Physics, Leeds Teaching Hospitals NHS Trust, UK
c) Department of Clinical Oncology, Leeds Teaching Hospitals NHS Trust, UK
d) Leeds Institute of Cancer and Pathology, University of Leeds, UK

Corresponding Author:

Dr Russell Frood, Research Fellow, Department of Nuclear Medicine, Level 1, Bexley Wing

St James's University Hospital, Beckett Street, Leeds, LS9 7TF, United Kingdom

Tel: +441132068212

Fax: +441132068228

Email: russellfrood@nhs.net

Running title: MR Textural Analysis in Oral Cavity Cancer

Word Count: 2585

Number of Figures: 2

Number of Tables: 5

Abstract

Objective: To explore the utility of MR texture analysis (MRTA) for detection of nodal extracapsular spread (ECS) in oral cavity squamous cell carcinoma (SCC).

Methods: 115 patients with oral cavity SCC treated with surgery and adjuvant (chemo)radiotherapy were identified retrospectively. First-order texture parameters (entropy, skewness and kurtosis) were extracted from tumour and nodal regions of interest (ROI) using proprietary software (TexRAD). Nodal MR features associated with ECS (flare sign, irregular capsular contour; local infiltration; nodal necrosis) were reviewed and agreed in consensus by two experienced radiologists. Diagnostic performance characteristics of MR features of ECS were compared with primary tumour and nodal MRTA prediction using histology as gold standard. Receiver operating characteristics (ROC) and regression analysis was also performed.

Results: Nodal entropy derived from contrast enhanced T1 weighted images was significant in predicting ECS ($p = 0.018$). MR features had varying accuracy: flare sign (71%); irregular contour (70%); local infiltration (66%); nodal necrosis (64%). Nodal entropy combined with irregular contour was the best predictor of ECS predictor ($p=0.004$, accuracy 79%). ECS was the only predictor of overall survival.

Conclusion: First-order nodal MRTA combined with imaging features may improve ECS prediction in oral cavity SCC.

Keywords

Magnetic Resonance Imaging; Mouth Neoplasms; Lymphatic Metastases

Key Points

1. Nodal MR textural analysis can aid in predicting extra capsular spread (ECS)
2. Nodal entropy was strongly significant in predicting ECS
3. Combining nodal entropy with irregular nodal contour improves predictive accuracy

Abbreviations

CET1-W	Contrast enhanced T1 weighted
ECS	Extra-capsular spread
MRTA	Magnetic Resonance Textural Analysis
MRI	Magnetic Resonance Imaging
SCC	Squamous Cell Carcinoma
T2-W	T2 weighted

Introduction

Oral cavity carcinoma affects approximately 260,000 people globally each year [1]. Over 90% of tumours affecting the oral cavity are squamous cell carcinoma (SCC) with the main risk factors being smoking and alcohol intake [2]. The new 8th Edition of the TNM Classification of Malignant Tumours includes nodal extracapsular spread (ECS) in staging criteria for the first time, with ECS spread leading to the majority of patients' disease being upstaged compared to patients with malignant lymph nodes without ECS [3]. This reflects the associated poor prognosis associated with ECS [4–6]. The current gold standard for detection of ECS is neck dissection and pathological staging.

The accuracy of pre-operative ECS detection varies between different imaging techniques with the mean sensitivity and specificity reported as 0.77 and 0.85 for CT, 0.85 and 0.84 for MRI and 0.87 and 0.75 for ultrasound with increasing accuracy in larger lymph nodes [7, 8]. Features on MRI associated with an increased likelihood of ECS include central necrosis, irregular contour, local infiltration and flare sign [9, 10].

There is increasing academic interest in extraction of additional quantifiable characteristics and features from imaging, referred to as radiomics. MRI textural analysis (MRTA) is an emerging application used to obtain additional non-visible imaging data for analysis using different statistical tests or models [11, 12]. One promising method applies filtered histogram analysis of extracted data and produces a range of first order parameters. These include entropy (a measure of disorder), kurtosis (how sharp the peak of the histogram is), skewness and mean [13]. These parameters do not take into consideration spatial relationship between pixels and therefore provide a more simplistic form of analysis which is less likely to be influenced by errors which can be introduced by different

scanners and scanning protocols [14]. Of these, entropy is the least likely to be influenced by variation in scanning parameters [14, 15].

The aim of this study was to compare diagnostic accuracy of traditional MRI features of ECS (central necrosis, irregular contour, local infiltration and flare sign) with first-order textural features (entropy, kurtosis and skewness) for predicting ECS in patients with known oral cavity carcinomas. Primary tumour textural features were also correlated with ECS status.

Materials and Methods

Ethical Considerations

Formal ethics approval or patient consent was not required as this was a retrospective data review and a waiver is granted at our institution in this circumstance.

Patient cohort

Patients with oral cavity SCC treated with surgery and (chemo)radiotherapy between 2008-16 with a pre-surgery MRI scan were retrospectively identified. 160 patients had MRI studies for oral cavity carcinoma during the study period. Of these 45 were excluded from the study due to no primary lesion being identified or artefact obscuring the lesion. 115 patients were included in the study (mean age 60 years, range 31-89 years, 73 (63%) males). Demographic data and pathology details were obtained from the institutional electronic patient record. All pre-surgery MRI scans were reviewed to determine whether any abnormal lymph nodes were present. For this purpose, an abnormal neck lymph node was defined as > 1cm in short axis, and/or with altered morphology or abnormal signal

characteristics. 73/115 patients were found to have abnormal lymphadenopathy on the pre-surgery MRI.

MRI technique

All MR imaging was performed using 1.5T MR scanners. The MR imaging protocols varied between manufacturers but included axial T1-weighted spin-echo images following an intravenous dose of 0.1mmol/kg of Gadolinium-based contrast and axial T2-weighted fast spin-echo images (**Table 1**).

Conventional MR image interpretation

The presence or absence of MR features associated with ECS (flare sign, irregular capsular contour, local infiltration, nodal necrosis) were independently assessed by two radiologists with a minimum of 7 years' experience of interpreting oncological head and neck MR imaging. Examples of the different MR features associated with ECS are depicted in **Figure 1**. Imaging was reviewed using an institutional picture archiving and communication system (PACS, Impax Version 6.5, Agfa Healthcare, Mortsel, Belgium). The radiologists were blinded to histological findings, there was moderate inter-observer agreement, $\kappa = 0.6$ $p = <0.001$. There were seven cases where there was a difference in opinion, these were then agreed in consensus.

MR Textural Analysis

Separate regions of interest (ROI) encompassing the largest nodal cross-sectional area and the primary tumour were defined on T2-weighted (T2-W) and post-contrast T1-weighted (CET1-W) images by two trainee radiologists under supervision by the two experienced radiologists. Cases were excluded if the primary tumour was not demonstrable on imaging, if images were significantly degraded by artefact

(motion/magnetic susceptibility artefact from dental amalgam) or if nodal size was less than 1cm in short axis. First-order texture parameters (entropy, skewness and kurtosis) were extracted from the ROIs using proprietary software (TexRAD, Cambridge Computing Ltd, UK) with fine (2mm), medium (4 mm) and coarse (6 mm) filters (**Figure 2**). The textural parameters were defined by the following equations:

$$Entropy = -\sum_{I=1}^{k} p(I) * log2(p(I))$$

$$Skewness = \sigma^{-3} \sum_{I=1}^{k} (\mathrm{I} - \mu)^3 \, p(I)$$

$$Kurtosis = \sigma^{-4} \sum_{I=1}^{k} (\mathrm{I} - \mu)^4 \, p(I) - 3$$

Where k reflects the grey level, σ is standard deviation, I is the intensity of the pixel value and P(I) is the probability of that pixel value occurring.

The filtration step employs a Laplacian of Gaussian band-pass spatial scale filter highlighting features at different widths (i.e. radii of 2mm, 4mm and 6mm). The filter sizes are independent to pixel size and therefore allow for integration of imaging features from fine to coarse (**Figure 3**). The first-order parameters mean, mean positive pixels (MPP) and standard deviation were excluded from analysis to mitigate against potential bias caused by signal intensity variation across different scanners and scanning protocols [14, 16]. Sub-centimetre lesions were not included due to possible sampling errors which have been reported in previous work assessing imaging textural analysis [17–19].

Statistical Analysis

Sensitivity, specificity, positive predictive value (PPV), negative predictive value (NPV) and accuracy of MR predictors of ECS were compared with histology as gold standard. MR textural analysis performance in predicting ECS was assessed using an independent t-test and Mann Whitney U test for non-parametric data. Correction for multiple testing was performed using the Holm-Bonferroni method. Areas under the curve (AUC) calculated by receiver operating characteristics (ROC) analysis and optimal threshold were calculated for texture parameters. Binary logistic regression was used to explore the relationship between the variables and ECS. Cox regression was used to evaluate predictors of survival. Multicollinearity was assessed via the variance inflation factor (VIF). All statistical analyses were performed using IBM SPSS Statistics (Version 22, IBM Corp, Amonk, NY, USA).

Results

Detailed patient characteristics are provided in **Table 2**. 45 of the 115-patient cohort (39%) had histologically proven ECS and 70 (61%) had no evidence of ECS on neck dissection histology (38 out of the 70 (54%) without ECS had metastatic lymph nodes at pathology). Of 115 patients included, 73 (63%) had measurable nodes (>1cm) on MR, 32 of these had ECS on histological examination. Importantly, 13 (31%) of the 42 patients with no measurable lymphadenopathy on pre-operative MRI demonstrated ECS on post-operative histology.

Analysis of first-order primary tumour textural features (n = 115) demonstrated no significant ability to predict the presence of ECS following correction for multiple testing (**Table 3**).

Analysis of first-order nodal textural features (n = 73) revealed that entropy extracted from nodal ROIs had a statistically significant correlation with ECS on CET1-W imaging independent of filtration level

when using independent T-test, corrected for multiple testing (**Table 4**). Entropy extracted with a medium-filter from CET1-W nodal ROIs demonstrated the most significance for predicting ECS (p=0.018, AUC = 0.7), with sensitivity 73%, specificity 53%, PPV 57%, NPV 69%, accuracy 60 % with a threshold > 5.26. Nodal kurtosis and skewness were not significant predictors of ECS (**Table 4**).

Of the 73 patients with measurable nodal disease, 13 (18%) demonstrated the flare sign (sensitivity 38%, specificity 95%, PPV 86%, NPV 66%, accuracy 70%), 42 (37%) demonstrated an indistinct capsular contour (sensitivity 69%, specificity 27%, PPV 42%, NPV 52%, accuracy 71%), 13 (18%) demonstrated infiltration of adjacent tissues (sensitivity 31%, specificity 93%, PPV 77%, NPV 63%, accuracy 66%) and 47 (41%) central nodal necrosis (sensitivity 72%, specificity 41%, PPV 49%, NPV 65%, accuracy 64%). All MRI characteristics demonstrated significance ($p < 0.05$) using a Fisher's exact test. Predictive performance of MRI characteristics and CET1-W nodal entropy are compared in **Table 5.**

Binary logistic regression was performed to determine the relationship between medium filter CET1-W and T2-W nodal entropy, fine filter T2-W primary tumour skewness and MR characteristics in the overall prediction of ECS. Each of the parameters were included in the model and the least significant was removed in a stepwise process until the only parameters remaining significantly contributed to the model. Both CET1-W entropy and the presence of an irregular nodal contour had a significant contribution to the model (Wald criteria $p = 0.01$ and $p = 0.004$ respectively) which itself was statistically significant in the prediction of ECS (chi square = 19.155, $p < 0.001$ with df = 2). The overall correct prediction being 79% (sensitivity 72%, specificity 84%, PPV 79%, NPV 78%, accuracy 79% (**Figure 4**)).

40 (of 115, 34.8%) patients died during the study period, with 21 (53%) having histological evidence of ECS. Cox regression was performed to assess the relationship between survival, age, perineural or lymphovascular spread, type of adjuvant treatment (chemoradiotherapy or radiotherapy) and medium filter T2-W primary tumour skewness. No parameter was significant in predicting survival outcome. Repeating the analysis for the 73 patients with measurable lymphadenopathy with inclusion of CET1-W and T2-W nodal entropy and MR characteristics again demonstrated no significant survival outcome prediction.

Discussion

Our results indicate that the use of CET1-W nodal entropy may aid in the prediction of ECS, and that combining this with more subjective imaging parameters such as the presence of an irregular nodal contour improves predictive accuracy. To the best of our knowledge the use of MRTA to predict ECS in oral cavity carcinoma patients has not previously been reported.

The presence of ECS in patients with oral cavity carcinoma is a significant prognostic indicator of poor outcome, associated with reduced 5-year survival rate, higher local recurrence rate and increased incidence of distant metastases [20]. Many previous studies have looked at the accuracy of different nodal imaging characteristics to correctly identify the presence of ECS with varying results. A meta-analysis by Su et al. assessed the accuracy of imaging features to determine ECS in patients with head and neck cancer, including nodal necrosis (sensitivity 80%, specificity 57%, accuracy 68%), local infiltration (sensitivity 50%, specificity 100%, accuracy 75%), irregular contour (sensitivity 50%, specificity 100%, accuracy 75%) and flare sign (sensitivity 77%, specificity 93%, accuracy 88%) [7]. More recent studies by Carlton et al. and Aiken et al. focussing on detection of ECS in patients with oral cavity cancer reported less impressive performance metrics for irregular contour (sensitivity 7-

48%, specificity 86-100%, accuracy 44-63%), infiltration into adjacent tissues (sensitivity 50%, specificity 84-86%, accuracy 63-65%) and nodal necrosis (sensitivity 63-64%, specificity 70-78%, accuracy 67-69%) [21, 22]. Randall et al. found the only imaging feature on CT which was statistically significant in predicting ECS in patients with oral cavity cancer was nodal necrosis (sensitivity 91%, specificity 50%, PPV 59%, NPV 88%) [23]. Prediction of ECS with MR defined characteristics in the current study was slightly better with flare sign (70%) and irregular contour (71%) having the best accuracy. This does highlight the need for an objective non-invasive prediction tool.

Nodal entropy extracted from CET1-W images (an objective measurement) had a significant correlation with ECS. Although this metric did not outperform subjective MR features, using binary logistic regression analysis the combination of CET1-W nodal entropy and presence of irregular nodal contour improved non-invasive prediction of ECS. This combination had the highest accuracy overall (79%).

The likelihood of detection of significant ECS has been demonstrated to increase as size of lymph nodes increases but it is also well recognised to occur in small nodes [5]. In this series 13 (29%) of 45 patients with ECS did not have measurable (<1cm) nodal disease on baseline imaging. Sub-centimetre lymph nodes were not analysed in our study due to concerns regarding possible sampling errors related to the spatial resolution of MRI. Previous PET and MR studies have also adopted this methodology [17–19]. There is currently a paucity of data analysing the effects of size of ROI on accuracy of MRTA. Hatt et al. concluded that textural features and metabolic volume complemented each other when volumes >10cm^3 were used which echoes concerns of partial voluming limiting accurate interpretation [18]. There remains an as yet unmet clinical need to reliably detect ECS in sub-centimetre nodes non-invasively. One approach might be to build a predictive model encompassing

primary tumour imaging phenotype. In this series, primary tumour skewness (fine filter) extracted from T2-W imaging was significant in predicting ECS but had poor accuracy (47%).

Textural features extracted from the primary tumour and nodal disease did not predict survival in this study. Seven of the patients who died had ECS with no measurable lymphadenopathy on MR which partly explains the findings that even though CET1-W nodal entropy and MRI characteristics had a significant ability to predict ECS they cannot significantly predict patient survival. Wreesman *et al*. reported a prognostic difference in how far tumour breached the nodal capsule with spread greater than 1.7mm having a worse prognosis [5]. This aspect was not evaluated in our study as the histological records for the patient cohort did not quantify the magnitude of ECS, a future study combining digital pathology with imaging could allow direct assessment of how nodal entropy correlates with extent of nodal capsular breach.

Our study was designed as a preliminary hypothesis generating study and consequently has several limitations, particularly the retrospective nature and imaging acquisition on different scanners. To mitigate against inherent variations in signal intensities between imaging data acquired on different scanners using similar but non-identical protocols, only three first order parameters: entropy, kurtosis and skewness were analysed. These three textural features reflect the shape and variation of imaging data rather than signal intensity differences; this should have limited the introduction of bias/sampling error. Ideally MR images should at least have the same slice thickness and field of view throughout the cohort of patients, with the spatial resolution being demonstrated to have a greater effect on variation of parameters when compared to repetition time, echo time and bandwidth [15, 24, 25]. The lack of standardised imaging protocols between institutes is a well-recognised limitation of retrospective radiomics research [25]. Predictive performance may improve with the inclusion of other MRI imaging sequences, including diffusion weighted imaging and should be explored in future

studies. The use of a single ROI which was performed by a single reader and agreed in consensus is also a limitation, as we were unable to analyse reproducibility of segmentation. Post-processing of MR data acquired from different scanners to erase inter-patient differences in intensity range, and resampling to a uniform matrix size has been shown to negate the effects of different MRI scanning protocols [26]. At present there is no agreed MRI harmonization method for multicentre radiomic analysis but this is the subject of current work by a number of groups. A recent review by Lambin et al. details key methodological steps and introduces the concept of a radiomics quality scoring system to try and improve the robustness of future textural analysis studies [27].

We chose to study oral cavity tumours as they are primarily treated surgically, and histology was therefore available for comparison. Non-invasive detection of ECS pre-surgery is unlikely to alter intended management in this patient cohort. Conversely, the ability to accurately predict presence of ECS on baseline imaging in more common types of head and neck squamous cell carcinoma, particularly oropharyngeal SCC, has the potential to guide treatment stratification and warrants further study. In the first instance, a controlled prospective study to validate our initial findings is required.

Conclusion

First order MRTA combined with imaging features may improve detection of ECS in oral cavity SCC. Further investigation is required to validate these initial results in a controlled prospective study.

References

1. Weatherspoon DJ, Chattopadhyay A, Boroumand S, Garcia I (2015) Oral cavity and oropharyngeal cancer incidence trends and disparities in the United States : 2000 – 2010.

Cancer Epidemiol 39:497–504 .

2. Llewellyn CD, Johnson NW, Warnakulasuriya KA (2001) Risk factors for squamous cell carcinoma of the oral cavity in young people: a comprehensive literature review. Oral Oncol 37:401-418

3. García J, López L, Bagué S, et al (2017) Validation of the pathological classification of lymph node metastasis for head and neck tumors according to the 8th edition of the TNM Classification of Malignant Tumors. Oral Oncol 70:29–33

4. Dünne AA, Müller HH, Eisele DW, Keßel K, Moll R, Werner JA (2006) Meta-analysis of the prognostic significance of perinodal spread in head and neck squamous cell carcinomas (HNSCC) patients. Eur J Cancer 42:1863–1868

5. Wreesmann VB, Katabi N, Palmer FL, et al (2016) Influence of extracapsular nodal spread extent on prognosis of oral squamous cell carcinoma. Head Neck 38:E1192–1199

6. Liao CT, Lee LY, Huang SF, et al (2011) Outcome Analysis of patients with oral cavity cancer and extracapsular spread in head and neck lymph nodes. Int J Radiat Oncol Biol Phys 81:930–937

7. Su Z, Duan Z, Pan W, et al (2016) Predicting extracapsular spread of head and neck cancers using different imaging techniques: a systematic review and meta-analysis. Int J Oral Maxillofac Surg 45:413–421

8. Chai RL, Rath TJ, Johnson JT, et al (2013) Accuracy of computed tomography in the prediction of extracapsular spread of lymph node metastases in squamous cell carcinoma of the head and neck. JAMA Otolaryngol Head Neck Surg 139:1187–1194

9. Kimura Y, Sumi M, Sakihama N, Tanaka F, Takahashi H, Nakamura T (2008) MR imaging criteria for the prediction of extranodal spread of metastatic cancer in the neck. AJNR Am J Neuroradiol 29:1355–1359

10. Lodder WL, Lange CA, van Velthuysen ML, et al (2013) Can extranodal spread in head and neck cancer be detected on MR imaging. Oral Oncol 49:626–633

11. Aerts HJ, Velazquez ER, Leijenaar RT, et al (2014) Decoding tumour phenotype by noninvasive imaging using a quantitative radiomics approach. Nat Commun 5:4006

12. Aggarwal N, Agrawal RK (2012) First and Second Order Statistics Features for Classification of Magnetic Resonance Brain Images. J Sign Process Syst 2012:146–153

13. Scalco E, Rizzo G (2017) Texture analysis of medical images for radiotherapy applications. Br J Radiol 90:20160642

14. Collewet G, Strzelecki M, Mariette F (2004) Influence of MRI acquisition protocols and image intensity normalization methods on texture classification. Magn Reson Imaging 22:81–91

15. Mayerhoefer ME, Szomolanyi P, Jirak D, Materka A, Trattnig S (2009) Effects of MRI acquisition parameter variations and protocol heterogeneity on the results of texture analysis and pattern discrimination: an application-oriented study. Med Phys 36:1236–1243

16. Sidhu HS, Benigno S, Ganeshan B, et al (2017) "Textural analysis of multiparametric MRI detects transition zone prostate cancer." Eur Radiol 27:2348–2358

17. Jalil O, Afaq A, Ganeshan B, et al (2017) Magnetic resonance based texture parameters as potential imaging biomarkers for predicting long-term survival in locally advanced rectal cancer treated by chemoradiotherapy. Colorectal Dis 19:349–362

18. Hatt M, Majdoub M, Vallieres M, et al (2015) 18F-FDG PET Uptake Characterization Through Texture Analysis: Investigating the Complementary Nature of Heterogeneity and Functional Tumor Volume in a Multi-Cancer Site Patient Cohort. J Nucl Med 56:38–44

19. Soussan M, Orlhac F, Boubaya M, et al (2014) Relationship between tumor heterogeneity measured on FDG-PET/CT and pathological prognostic factors in invasive breast cancer. PLoS

One 9:e94017

20. Shaw R, Stat D, Woolgar J, et al (2010) Extracapsular spread in oral squamous cell carcinoma. Head Neck 32:714–722

21. Carlton JA, Maxwell AW, Bauer LB, et al (2017) Computed tomography detection of extracapsular spread of squamous cell carcinoma of the head and neck in metastatic cervical lymph nodes. Neuroradiol J 30:222–229

22. Aiken AH, Poliashenko S, Beitler JJ, et al (2015) Accuracy of preoperative imaging in detecting nodal extracapsular spread in oral cavity squamous cell carcinoma. Am J Neuroradiol 36:1776–1781

23. Randall D, Lysack JT, Hudon ME, et al (2015) Diagnostic utility of central node nerosis in predicting etracapsular spread among oral cavity squamous cell carcinoma. Head Neck 37:92–96

24. Kumar V, Gu Y, Basu S, et al (2012) Radiomics: The process and the challenges. Magn Reson Imaging 30:1234–1248

25. Sala E, Mema E, Himoto Y, et al (2017) Unravelling tumour heterogeneity using next-generation imaging: radiomics, radiogenomics, and habitat imaging. Clin Radiol 72:3–10

26. Fortin JP, Parker D, Tunç B, et al (2017) Harmonization of multi-site diffusion tensor imaging data. Neuroimage 161:149–170

27. Lambin P, Leijenaar RTH, Deist TM, et al (2017) Radiomics: The bridge between medical imaging and personalized medicine. Nat Rev Clin Oncol 14:749–762

Tables and Figures

Table 1: The parameters used in the different scanner protocols within the study

	Siemens						**Philips**				**GE**	
	Protocol 1		**Protocol 2**		**Protocol 3**		**Protocol 1**		**Protocol 1**			
	CET1	**T2**	**CET1**	**T2**	**CET1**	**T2**	**CET1**	**T2**	**CET1**	**T2**	**CET1**	**T2**
Repetition time (ms)	600	10450	770	5940	615	6400	700	4900	790	6230	710	7940
Echo Time (ms)	11	80	22	92	13	116	15	110	15	120	12	80
Echo Train	3	13	2	13	3	13	5	20	4	15	3	26
Band width (Hx/pixel)	305	200	200	190	250	120	370	195	273	109	244	195
Field of view	240x240	200x200	180x180	180x180	250x250	250x250	230x230	230x230	230x230	230x230	240x240	240x240
Slice Thickness (mm)	3	3.5	5	5	4	4	5	5	5	5	6	6
Slice Gap (mm)	1	1	1	1	1	1	1	1	1	1	1	1
Base Matrix	256x166	320x192	256x192	256x192	320x244	320x208	208x167	368x290	256x204	368x293	320x256	352x352
Pixel size (mm)	0.9x1.4	0.6x1.0	0.7x0.9	0.7x0.9	0.8x1.0	0.8x1.2	0.89 x1.4	0.48 x0.8	0.89 x1.1	0.5x0.8	0.8x0.9	0.7

Key: CET1 = Contrast-enhanced T1-weighted sequence, T2 = T2-weighted sequence

Table 2: Baseline characteristics and demographics of the patient cohort

Gender	
Male	73 (63%)
Female	42 (37%)
Age (Mean, +/- range)	60 years (31-89 years)
Scanner imaging performed	
Siemens Protocol 1	57 (50%)
Siemens Protocol 2	10 (9%)
Siemens Protocol 3	9 (8%)
Philips Protocol 1	8 (7%)
Philips Protocol 2	20 (17%)
GE Protocol	11 (10%)
Primary Site	
Lip	2 (2%)
Anterior 2/3rd of the tongue	59 (51%)
Buccal Mucosa	9 (8%)
Alveolus	4 (3%)
Retromolar Trigone	14 (12%)
Floor of the mouth	27 (23%)
T stage (pathological)	
T1	12 (10%)
T2	47 (41%)
T3	15 (13%)
T4a	40 (35%)
T4b	1 (1%)
N Stage (pathological)	
N0	33 (29%)
N1	25 (22%)
N2a	0
N2b	50 (43%)
N2c	7 (6%)

N3	0
ECS	
Positive	45 (39%)
Negative	70 (61%)
Lymphovascular Spread	
Positive	51 (44%)
Negative	64 (56%)
Perineural Spread	
Positive	62 (54%)
Negative	53 (46%)
Adjuvant Treatment	
Chemoradiotherapy	35 (30%)
Radiotherapy	76 (66%)
Declined	4 (4%)
Follow up	
Alive	75 (65%)
Deceased	40 (35%)

Table 3: Correlation between primary tumour first order textural parameters and ECS

Textural Parameter	MR Sequence	Filter size (mm)	Extracapsular Spread		No Extracapsular spread		P value	Corrected P value
			Mean	**SD**	**Mean**	**SD**		
Entropy	T1	2	6.12	0.73	6.11	0.65	0.926	
	T1	4	6.19	0.77	6.16	0.68	0.872	
	T1	6	6.20	0.79	6.16	0.67	0.817	
	T2	2	6.17	0.70	6.15	0.57	0.881	
	T2	4	6.20	0.72	6.18	0.58	0.858	
	T2	6	6.18	0.74	6.17	0.60	0.955	
Skewness	T1	2	0.15	0.53	0.22	0.59	0.510	
	T1	4	-0.09	0.56	-0.10	0.56	0.948	
	T1	6	-0.23	0.47	-0.26	0.57	0.784	
	T2	2	0.28	0.51	0.54	0.66	0.025*	0.45
	T2	4	0.05	0.50	0.19	0.61	0.213	
	T2	6	-0.04	0.42	0.37	0.56	0.443	
Kurtosis	T1	2	0.36	1.82	0.53	1.46	0.794	
	T1	4	-0.04	1.13	-0.02	0.97	0.614	
	T1	6	-0.17	0.88	-0.66	1.1	0.233	
	T2	2	0.37	0.99	0.77	2.26	0.069	
	T2	4	-0.23	0.95	0.02	1.36	0.504	
	T2	6	-0,24	0.84	-0.18	0.83	0.866	

Key: T1 = Contrast-enhanced T1-weighted imaging, T2 = T2-weighted imaging,

* = $p < 0.05$. Values for kurtosis represent median and IQR. The corrected P value was calculated using the Holm-Bonferroni method.

Table 4: Correlation between nodal first order textural parameters and ECS

Textural Parameter	MR Sequence	Filter size (mm)	Extracapsular Spread		No Extracapsular spread		P value	Corrected P value
			Mean	SD	Mean	SD		
Entropy	T1	2	5.76	0.77	5.20	0.78	0.003*	0.051
	T1	4	5.81	0.78	5.18	0.78	0.001*	0.018*
	T1	6	5.81	0.79	5.23	0.81	0.003*	0.051
	T2	2	5.85	0.77	5.50	0.55	0.037*	0.481
	T2	4	5.89	0.75	5.48	0.57	0.013*	0.195
	T2	6	5.87	0.75	5.46	0.57	0.013*	0.195
Skewness	T1	2	-0.04	0.39	-0.18	0.40	0.778	
	T1	4	-0.44	0.44	-0.19	0.33	0.124	
	T1	6	-0.11	0.31	-0.24	0.33	0.092	
	T2	2	0.10	0.48	0.74	0.46	0.832	
	T2	4	-0.002	0.39	0.013	0.52	0.894	
	T2	6	-0.05	0.46	0.02	0.47	0.561	
Kurtosis	T1	2	**-0.39**	**0.69**	**-0.40**	**0.73**	0.450	
	T1	4	**-0.52**	**0.97**	**-0.63**	**0.71**	0.308	
	T1	6	**-0.80**	**0.56**	**-0.72**	**0.71**	0.322	
	T2	2	**-0.34**	**0.76**	**-0.30**	**0.72**	0.748	
	T2	4	**-0.62**	**0.65**	**-0.58**	**0.68**	0.880	
	T2	6	**-0.76**	**0.46**	**-0.82**	**0.55**	0.417	

Key: T1 = Contrast-enhanced T1-weighted imaging, T2 = T2-weighted imaging,

* = p <0.05. Values for kurtosis represent median and IQR. The corrected P value was calculated using the Holm-Bonferroni method.

Table 5: Comparison of diagnostic performance characteristics for detection of ECS of different textural parameters and MRI imaging features

Parameter	Sensitivity (%)	Specificity (%)	PPV (%)	NPV (%)	Accuracy (%)
CET1-W Nodal Entropy (5.26) – medium filter	72	54	56	69	60
Flare sign	38	95	86	66	70
Indistinct capsular contour	69	27	42	52	71
Infiltration of adjacent tissues	31	93	77	63	66
Central necrosis	72	41	49	65	64

Key: CET1-W = Contrast-enhanced T1-weighted imaging, T2-W = T2-weighted imaging, ( ) = threshold value.

Figure 1: Axial T2- and T1-weighted contrast enhanced images depicting MR features associated with extracapsular noda spread (ECS) including flare sign (white arrow), irregular nodal contour (white arrowhead), central nodal necrosis (red arrow) and soft tissue infiltration (red arrowhead)

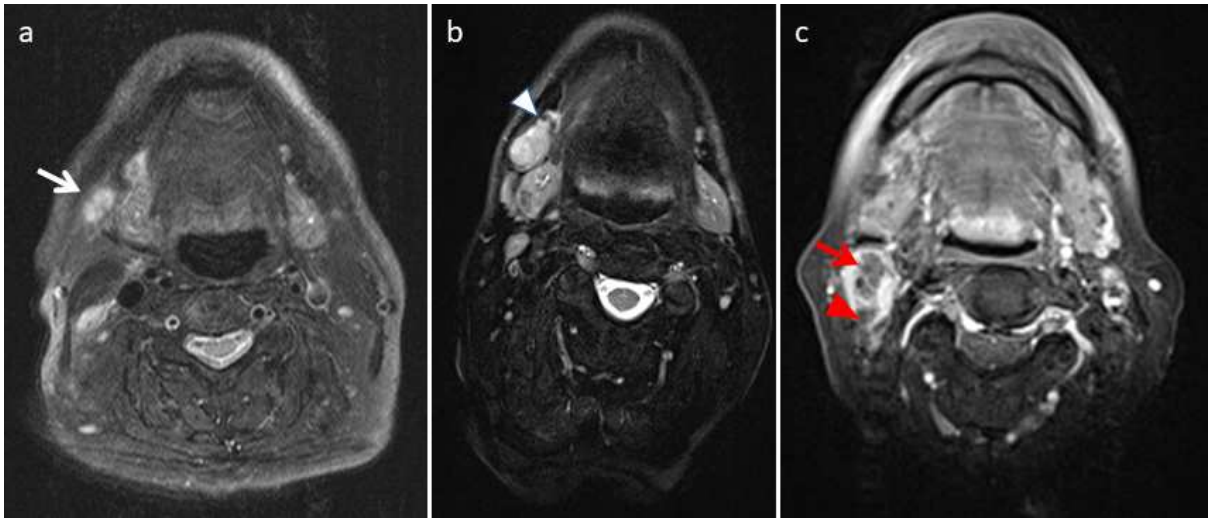

Figure 2: Screenshot from TexRad demonstrating a region of interest drawn around a left level 2 lymph node on an axial fat-suppressed T2-weighted image with the associated histogram of measured intensities

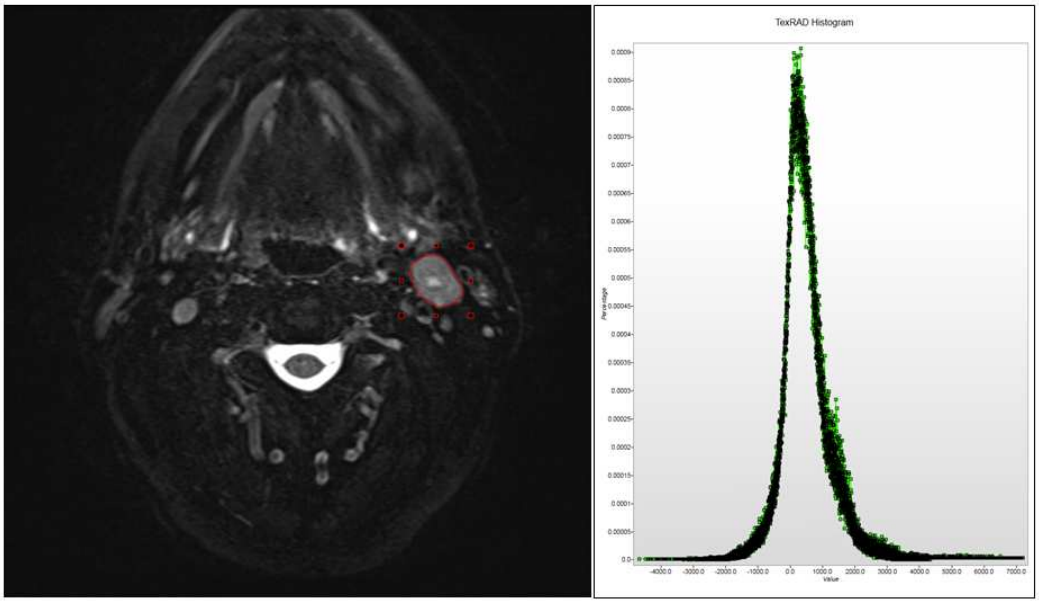

Figure 3: Screenshot from TexRad demonstrating a region of interest (ROI) drawn around a right level 2 lymph node on a fat-supressed T1-weighted contrast enhanced image (a) with the corresponding segmented ROI with fine (2mm), medium (4mm) and coarse (6mm) filters applied (b, c and d respectively)

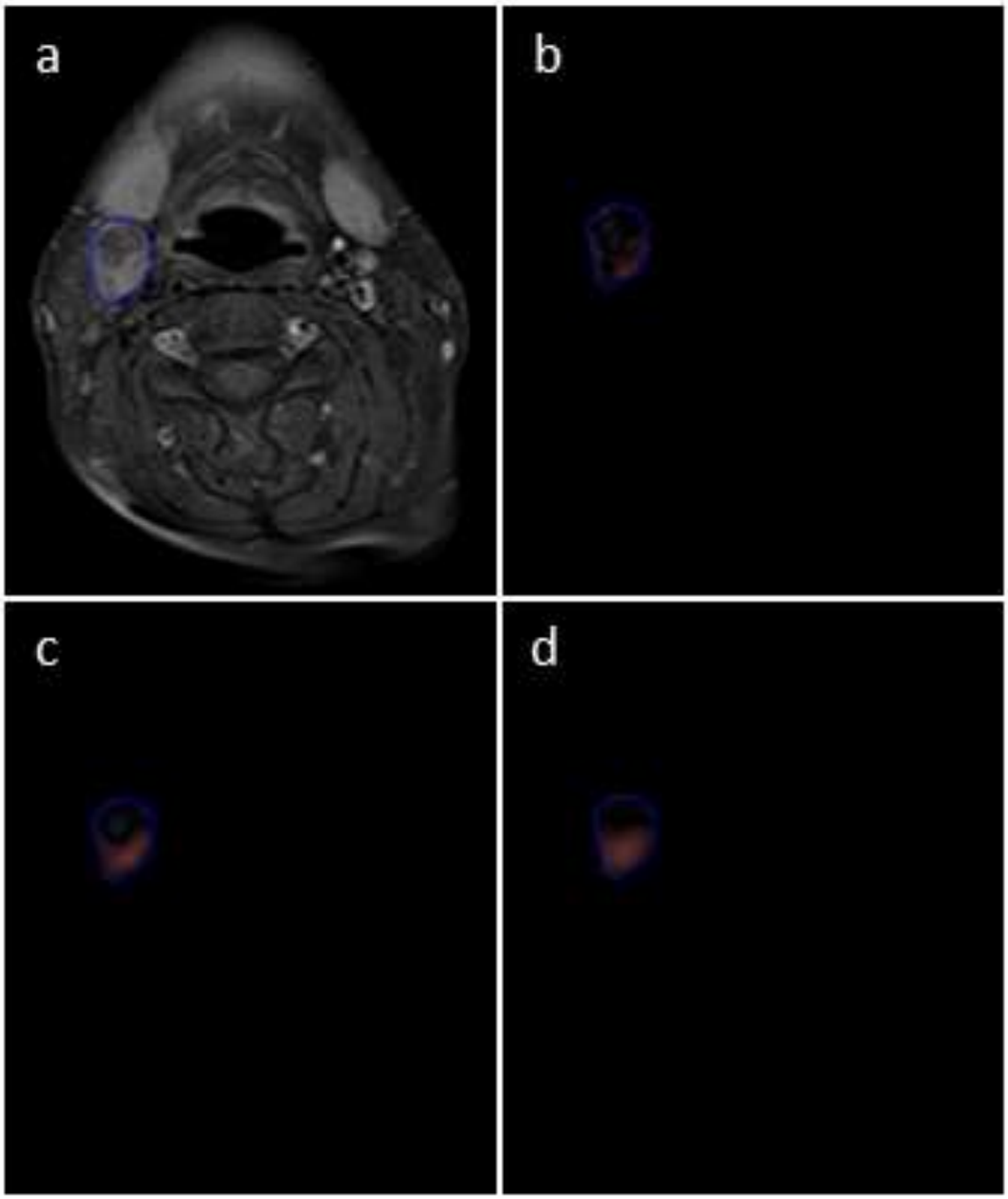

Figure 4: Receiver Operating Characteristics (ROC) curve for the CET1-W and MR irregular contour model's ability to predict ECS

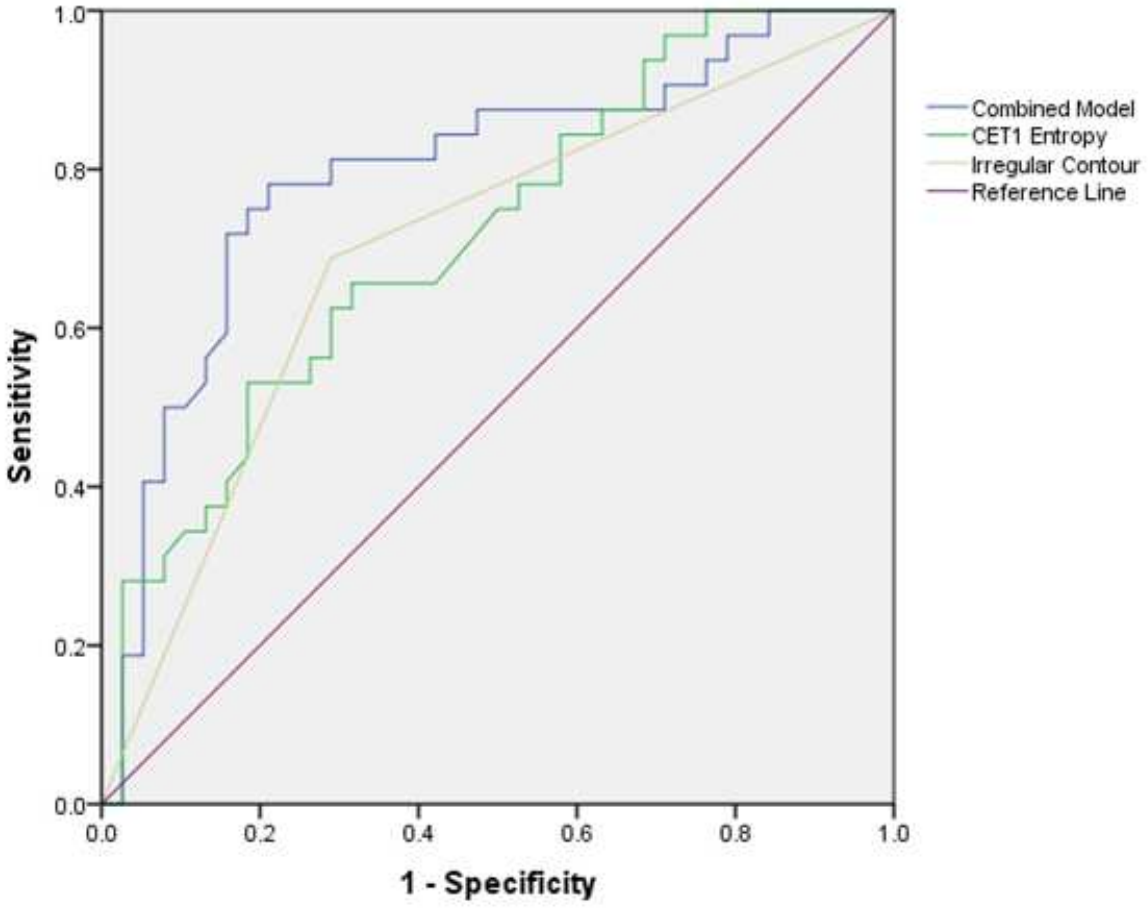

Key: CET1-W – contrast-enhanced T1-weighted